




Tuning plasmonic nanostructures in graphene-based nano-sandwiches using ultraviolet/ozone functionalization

Dai Zhang¹, Ying Du¹, Cheng Yang¹, Pan Zeng¹, Yan Yu¹, Yujun Xie¹, Rongqing Liang¹, Qiongrong Ou^{1,*}, and Shuyu Zhang^{1,*} 

¹Department of Light Sources and Illuminating Engineering, and Academy for Engineering and Technology, Institute for Electric Light Sources, Fudan University, Shanghai 200433, China

Received: 22 June 2020

Accepted: 19 September 2020

Published online:
29 September 2020

© Springer Science+Business
Media, LLC, part of Springer
Nature 2020

ABSTRACT

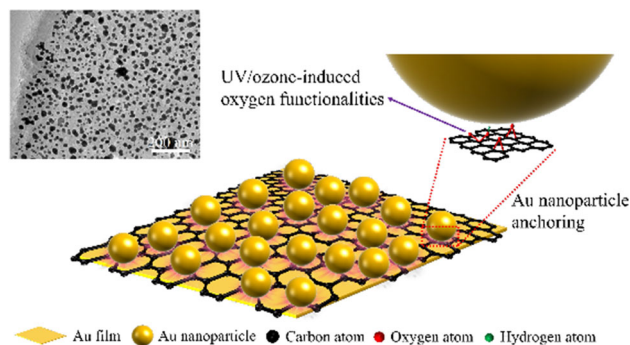
Graphene-based plasmonic sandwiches have received considerable research interest because of their intriguing optical, electronic and catalytic properties. The capability of tuning the distribution of plasmonic nanostructures is essential for exploring their intrinsic properties and potential applications. Herein, we report an ultraviolet (UV)/ozone-assisted approach to synthesizing gold nanoparticles/reduced graphene oxide/gold thin film (AuNPs/RGO/Au) plasmonic nano-sandwiches with easy and fine tunability of AuNPs at room temperature. The UV/ozone functionalization controls the activation of anchor sites for AuNPs on the GO scaffold without creating new defects on the basal plane. By simply varying the functionalization time, the loading density of AuNPs with an average size of ~ 17 nm is able to reach a value of over $500 \mu\text{m}^{-2}$, which is higher than previously reported values using other room-temperature methods. The AuNPs/RGO/Au plasmonic nano-sandwiches offer remarkable near-field enhancement with an enhancement factor of over 300 in the Raman signal of graphene, which is comparable with the highest reported values. The as-prepared AuNPs/RGO/Au nano-sandwiches can be used as sensitive surface-enhanced Raman spectroscopy substrates. This work demonstrates that oxygen-containing functional groups, which were commonly considered to have negative effects on graphene-based nanocomposites, can contribute to the successful synthesis of high-loading plasmonic nano-sandwiches.

Handling Editor: Pedro Camargo.

Address correspondence to E-mail: qrou@fudan.edu.cn; zhangshuyu@fudan.edu.cn

<https://doi.org/10.1007/s10853-020-05376-x>

GRAPHIC ABSTRACT



Introduction

Functionalizing graphene with metal nanoparticles (NPs) has been demonstrated as an effective way to broaden its range of applications [1–7]. Among them, graphene-based plasmonic nano-sandwiches, which consist of two layers of metal components with a layer of graphene or its derivatives intercalated between them, have drawn tremendous research interest in the field including optoelectronics [8–10], energy conversion/storage [11, 12] and sensing [13–15]. In practical applications, it is of critical importance to have the capability of tuning the size and loading density of metal NPs [16] during the fabrication stage, since it determines the performance of plasmonic nano-sandwiches [1, 17]. So far, a variety of high-throughput synthetic strategies has been proposed, which can be categorized into *ex situ* hybridization and *in situ* crystallization [18, 19]. The *ex situ* hybridization employs self-assembly of pre-synthesized metal NPs onto the surfaces of graphene oxide (GO) or reduced graphene oxide (RGO) in solutions. Although *ex situ* hybridization has good control over sizes and shapes of metal NPs, it has much less control over their loading density and distribution uniformity on the surfaces [20–22]. The *in situ* crystallization provides on-site growth or formation of metal NPs by chemical reduction or thermal evaporation, but the toxicity of reducing agents [23, 24] or the high temperature of thermal annealing [15, 25] triggers its incompatibility with

flexible optoelectronics and thus limits the application scenarios.

Plasma technology has been demonstrated as an efficient approach to fabricating metal or alloy composites on various supports [26–29] at room temperature without introducing organic impurities or unwanted byproducts. Since the oxygen functional groups act as the nucleation sites of the metal NPs when GO is used as the support material [19, 30], the quantity control of these oxygenated groups holds the potential to achieve graphene-based plasmonic nano-sandwiches with high metal-NPs loadings.

Inspired by this idea, we report, in this paper, a synthetic strategy to fabricate gold nanoparticles/reduced graphene oxide/gold thin film (AuNPs/RGO/Au) plasmonic nano-sandwiches using a combination of UV/ozone functionalization and argon (Ar) plasma reduction. The large amount of additional oxygen-containing functional groups induced by UV/ozone treatment, which were generally associated with negative contributions, are now utilized to modulate the nucleation and growth processes of AuNPs on the surfaces of RGO and achieve high-loading plasmonic nano-sandwiches. The density of AuNPs with an average size of ~ 17 nm can reach a value of over $500 \mu\text{m}^{-2}$. The AuNPs/RGO/Au plasmonic nano-sandwiches offer significant near-field enhancement and effectively enhance Raman signals from graphene by over 300 fold. We further explored the applications of the as-prepared plasmonic nano-sandwiches as sensitive SERS substrates. Compared with the traditional plasma reduction method

[31, 32], our strategy offers an effective solution to achieving much denser metal NPs, and at the same time significantly alleviates the etching effect of plasma.

Materials and methods

Reagents and materials

All reagents were of analytical grade and used as received without further purification. Graphite oxide powder was purchased from Jiangsu XFNANO Materials Tech Co., Ltd (Nanjing, China). Chloroauric acid ($\text{HAuCl}_4 \cdot 3\text{H}_2\text{O}$, $\geq 99.9\%$) and Rhodamine 6G (R6G, 99%) were purchased from Aladdin reagent (Shanghai, China). Acetone and isopropanol (IPA) were supplied by Sinopharm Chemical Reagent Co., Ltd (Shanghai, China). Silicon (Si) wafers with a 300-nm-thick oxide layer (SiO_2) were obtained from Suzhou Crystal Silicon Electronic & Technology Co., Ltd (Suzhou, China).

Preparation of $\text{HAuCl}_4/\text{GO}/\text{Au}$ thin film on the SiO_2/Si wafer

A 50-nm-thick Au film was first deposited onto the SiO_2/Si wafer by electron-beam evaporating using a Combinatorial Materials Science Platform (Kurt J. Lesker Company). The substrate was then cut into 1×1 cm wafers for further processing. A 0.5 mg mL^{-1} GO aqueous dispersion was prepared by sonicating GO powder (15 mg) in deionized water (30 ml) for 30 min. The Au film was firstly treated with UV/ozone (PSD Series, Digital UV Ozone system, Novascan Technologies, Inc) for 60 min to improve the hydrophilicity. Then, 50 μl GO aqueous solution was drop-casted onto the Au thin film, and the wafers were naturally dried overnight. The GO-coated Au thin film was again treated with UV/ozone for 30 min, 60 min, 90 min, 120 min, 150 min and 180 min, respectively. 118.149 mg chloroauric acid powder was dissolved in 30 ml IPA to make a 10 mM solution. A droplet of 10 μl HAuCl_4 solution was drop-casted onto each UV/ozone-treated GO-coated Au thin film, and the solvent was evaporated in air.

Reduction of HAuCl_4 and GO by Ar plasma

The Ar plasma reaction was implemented in a custom-made plasma system using a radio frequency inductively coupled plasma (ICP). The detailed configuration has been reported in our previous work [33]. The chamber was sequentially evacuated by mechanical and turbo molecular pumps to 1.0×10^{-3} Pa before the generation of Ar plasma. The flow rate of pure Ar was controlled at 100 standard cubic centimeter per minute (sccm) and Ar plasma was generated at 4.0 Pa with an ICP frequency of 13.56 MHz and a power supply of 88 W. The length of Ar plasma reduction was fixed at 15 min, which we found is the optimal condition to obtain small and dense AuNPs. Plasma serves as the dual “reducing agent” for GO and Au^{3+} [27]. The as-prepared AuNPs/RGO/Au nano-sandwiches with UV/ozone treatment time length of 30 min, 60 min, 90 min, 120 min, 150 min and 180 min was labeled as S1, S2, S3, S4, S5 and S6, respectively. For comparison, we also fabricated AuNPs/RGO/Au nano-sandwiches using pristine GO (corresponding to UV/ozone treatment for 0 min), which was labeled as S0.

Microscopic characterization of AuNPs/RGO/Au nano-sandwiches

The GO films before and after the UV/ozone treatment were characterized by X-ray photoelectron spectroscopy (XPS, PHI-5300, Ulvac Phi Inc.). For XPS analyses, 50 μl GO dispersion was drop-casted onto Au/ SiO_2/Si substrates that were firstly treated with UV/ozone for 60 min. The as-casted samples were dried overnight in air and treated with UV/ozone for 0 min, 60 min, 120 min and 180 min, respectively. XPS deconvolution processing was conducted on AugerScan software. The peak positions of non-oxygenated carbon (C–C/C=C), hydroxyl (C–O), carbonyl (C=O) and carboxyl (O–C=O) were fixed at 284.6 eV, 286.1 eV, 287.3 eV and 288.7 eV, respectively. The morphology of AuNPs/RGO/Au nano-sandwiches was characterized using a field emission scanning electron microscopy (FESEM, merlin compact, Carl Zeiss, Germany). The structure of AuNPs/RGO was analyzed using transmission electron microscopy (TEM, Tecnai G2 20-s-twin, FEI, America). To prepare the sample for the TEM characterization, 50 μl GO solution was drop-casted onto a fused silica substrate. Before the drop-casting

process, the fused silica substrate was sequentially cleaned by sonication in bath of acetone, IPA and deionized water for 15 min each and the glass substrate was then treated with UV/ozone for 15 min to improve the surface hydrophilicity. The as-deposited sample was dried overnight in air at room temperature to form a GO film, followed by UV/ozone for 120 min. Then, 10 μl HAuCl_4 solution was drop-casted onto the UV/ozone-treated GO film, and the identical Ar plasma reduction process was performed as described above. The AuNPs/RGO film separated from the substrate by immersing the as-prepared sample into an ethanol solution and was subsequently transferred onto a copper grid.

SERS measurements

Raman spectra were obtained using a Renishaw in Via Raman system with a 633 nm laser. The laser power was kept at 1.7 mW to avoid overheating. The accumulation time was set as 10 s. The numerical aperture was 0.5, and the objective was $\times 50$. The parameters were identical for all measurements. For each sample, we recorded three Raman spectra in different positions and took the average values. To investigate the enhancement of Raman signal of graphene in the AuNPs/RGO/Au plasmonic nano-sandwiches, Raman spectra of GO spin-coated on SiO_2/Si , GO spin-coated on $\text{Au}/\text{SiO}_2/\text{Si}$ and AuNPs/RGO/Au nano-sandwiches were recorded. For assessment of the performance of our AuNPs/RGO/Au plasmonic nano-sandwiches as SERS substrates, R6G was used as the standard probe molecule. Before the measurements, a droplet of 10 μl R6G solution was dropped onto each sample, and the solvent was evaporated in a vacuum oven at room temperature.

Raman analyses of GO film

To investigate the structural change of GO during the process of UV/ozone treatment, we conducted Raman analyses of GO films treated with UV/ozone for different time lengths. To avoid the depth-average effect during the Raman measurements, we prepared GO films by spin-coating the GO dispersion on $\text{Au}/\text{SiO}_2/\text{Si}$ substrates at 2000 rpm for 30 s. Prior to the spin-coating, the $\text{Au}/\text{SiO}_2/\text{Si}$ substrates were pre-treated with UV/ozone for 60 min. After the spin-

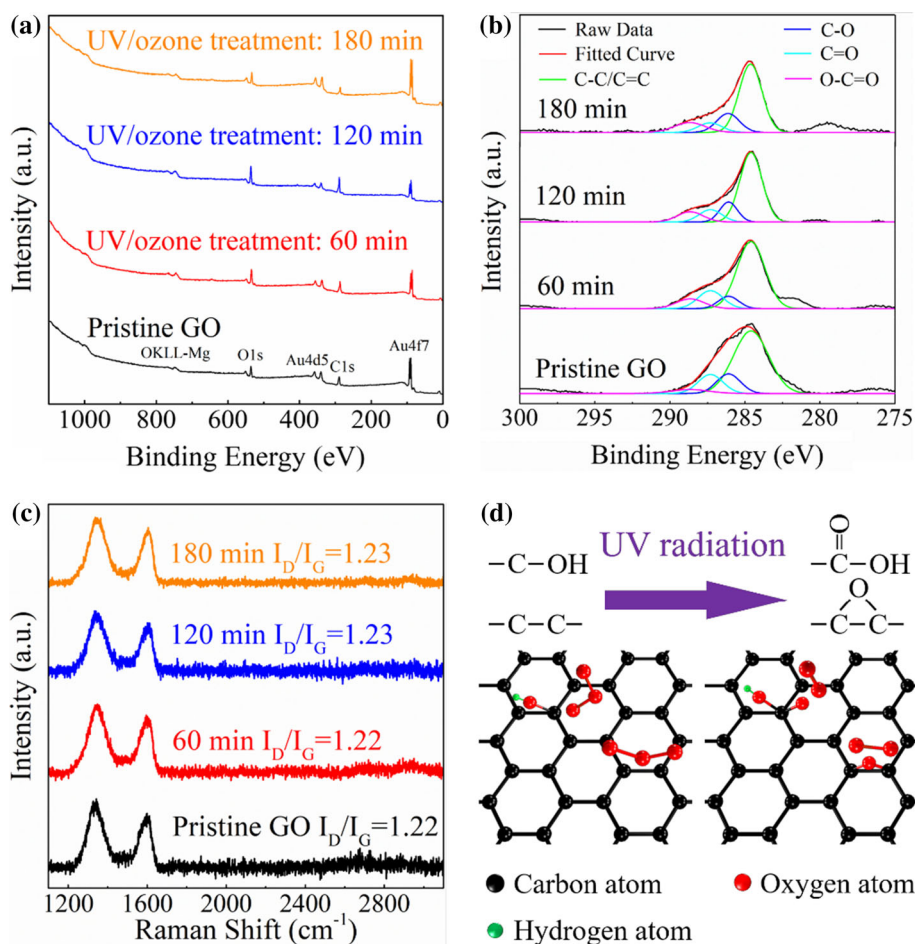
coating the GO films were treated with UV/ozone for 0 min, 60 min, 120 min and 180 min, respectively.

Results and discussion

Functionalization of GO via UV/ozone treatment

The XPS survey spectra of pristine GO film and GO films treated with UV/ozone for 60 min, 120 min and 180 min are shown in Fig. 1a, and the corresponding chemical composition is listed in Table 1. It can be seen that the ratios of C:O decreased as we prolonged UV/ozone treatment, indicating UV/ozone treatment will raise the oxidation degree of GO sheets. Figure 1b illustrates the high-resolution C1s spectra of GO treated with UV/ozone for 0 min (pristine), 60 min, 120 min and 180 min, respectively. The C1s spectrum of pristine GO can be deconvoluted into four components: non-oxygenated carbon (C–C/C=C), hydroxyl (C–O), carbonyl (C=O) and carboxyl (O–C=O) [34, 35], and the peak energies are calibrated by assigning the major C1s peak at 284.6 eV [36]. The changes of chemical bonding of GO during the UV/ozone treatment process are listed in Table 2, revealing that UV/ozone treatment can effectively increase the oxygen-containing functional groups on the GO basal plane. For UV/ozone-treated GO, it has been proposed that ozone molecules can be first physisorbed on the graphene basal plane with a binding energy of 0.25 eV and then be dissociated into an epoxide group (C–O–C) and a separate oxygen molecule [37]. Since C–O–C bonds typically exhibit a binding energy of ~ 286 eV [38, 39] which is very close to that of C–O bonds and can lead to an almost utter overlap of these two components in the C1s spectrum, the overall percentage of C–O/C–O–C bonds slightly decreased during the first 60 min of UV/ozone treatment and then steadily increased with a much faster pace if the UV/ozone treatment continued. In addition, the content of O–C=O bonds grew progressively due to UV/ozone exposure, which agrees with previous studies [40, 41]. We believe that they were created mainly through the oxidation of C–O moieties into O–C=O moieties under the conditions of UV radiation and existence of ozone, which explains the fact that the C–O/C–O–C proportion decreased at first when the time length of UV/ozone treatment was 60 min or less. This also

Figure 1 **a** XPS survey spectra, **b** the high-resolution C1s deconvolution spectra and **c** Raman spectra of GO treated with UV/ozone for 0 min, 60 min, 120 min and 180 min, respectively. **d** Schematic illustration showing the mechanism of functionalizing GO by UV/ozone.



explains why the O–C=O proportion reached a plateau when the treatment time reached 120 min or above, while the C–O/C–O–C proportion did not: the formation of O–C=O moieties required the

consumption of C–O moieties and the condition of UV/ozone, whereas the formation of C–O–C moieties only needed the latter.

Table 1 The compositional changes of GO with increasing UV/ozone treatment time

<i>t</i> (min)	C (%)	O (%)	Au (%)	C/O
0	65.10	22.20	12.70	2.93
60	63.50	28.77	7.73	2.21
120	65.14	29.78	5.07	2.18
180	52.87	27.62	19.5	1.91

Figure 1c demonstrates the Raman spectra of GO treated with UV/ozone for 0 min (pristine), 60 min, 120 min and 180 min. The four spectra exhibit a similar pattern: a D band centered at ~ 1350 cm⁻¹ and a G band centered at ~ 1600 cm⁻¹. The intensity ratio of D- and G-band (I_D/I_G) has been used as an indicator of degradation degree of crystallinity of graphitic materials and an increase in I_D/I_G means more defects on the GO basal plane [42–44]. The value of I_D/I_G of GO treated with UV/ozone for 0 min, 60 min, 120 min, 180 min was calculated to be

Table 2 The trend of chemical bonding in GO with increasing UV/ozone treatment time

<i>t</i> (min)	C–C/C=C (%)	C–O/C–O–C (%)	C=O (%)	O–C=O (%)
0	66.9	14.1	14.4	4.6
60	65.8	8.9	15.7	9.6
120	63.5	14.4	11.4	10.7
180	61.9	17.0	9.1	12.0

1.23 ± 0.03 , 1.23 ± 0.03 , 1.22 ± 0.02 , 1.22 ± 0.03 , respectively. This indicates the process of UV/ozone exposure did not create new defects in GO. Along with the findings of XPS analyses, we can conclude that the formation of oxygen functionalities during the UV/ozone treatment process preferentially occurred at the existing defective sites, that is to say, O–C=O moieties were formed at the former C–O sites and the formation of C–O–C moieties did not require breaking C=C/C–C bonds on the GO basal plane. Figure 1d summarizes the proposed reaction mechanism of GO with ozone under UV radiation.

Morphology of AuNPs/RGO/Au nano-sandwiches

Figure 2a–g shows the SEM images of AuNPs/RGO/Au nano-sandwiches with UV/ozone treatment time increasing from 0 min to 180 min, and Fig. 2h summarizes the changes of particle size and density as a function of the UV/ozone treatment time. The average size of AuNPs on the top of AuNPs/RGO/Au nano-sandwiches was measured to be 20 ± 7 nm, 22 ± 6 nm, 19 ± 7 nm, 16 ± 5 nm, 17 ± 5 nm, 36 ± 17 nm, 78 ± 43 nm, respectively. The density of AuNPs on the surface of RGO with 0 min, 30 min, 60 min, 90 min, 120 min, 150 min and 180 min of UV/ozone treatment was $40 \pm 11 \mu\text{m}^{-2}$, $61 \pm 12 \mu\text{m}^{-2}$, $105 \pm 12 \mu\text{m}^{-2}$, $272 \pm 10 \mu\text{m}^{-2}$, $508 \pm 9 \mu\text{m}^{-2}$, $293 \pm 60 \mu\text{m}^{-2}$ and $143 \pm 127 \mu\text{m}^{-2}$, respectively. It is evident that the density of AuNPs increased significantly as the treatment time increased from 0 to 120 min. Yet the density did not continue to rise but declined dramatically, and the particles tended to merge and exhibited island-like morphology when the treatment time reached 150 min or above (corresponding to S5 and S6). This indicates that when GO was treated with UV/ozone for a reasonable amount of time, the increased oxygen functional groups can adsorb gold ions through physisorption, electrostatic binding, or charge-transfer interactions [23] and then serve as nucleation sites for gold ions anchoring during the subsequent argon plasma reduction process [45]. However, the oxygen functional groups can become over-concentrated due to excessive UV/ozone treatment so that the spacing between Au nuclei is narrowed, which consequently leads to the aggregation of AuNPs and the island-like morphology.

The change in particle size has an impact on the plasmonic properties of AuNPs/RGO/Au nano-sandwiches. We measured the reflection spectra of AuNPs/RGO/Au nano-sandwiches with UV/ozone treatment of 0 min, 60 min, 120 min and 180 min, respectively (corresponding to the sample of S0, S2, S4 and S6, respectively), and the peak was red-shifted with the increased of particle size (Fig. S1). The percentage of AuNPs covering each AuNPs/RGO/Au nano-sandwich is shown in Fig. S2 in the supporting information.

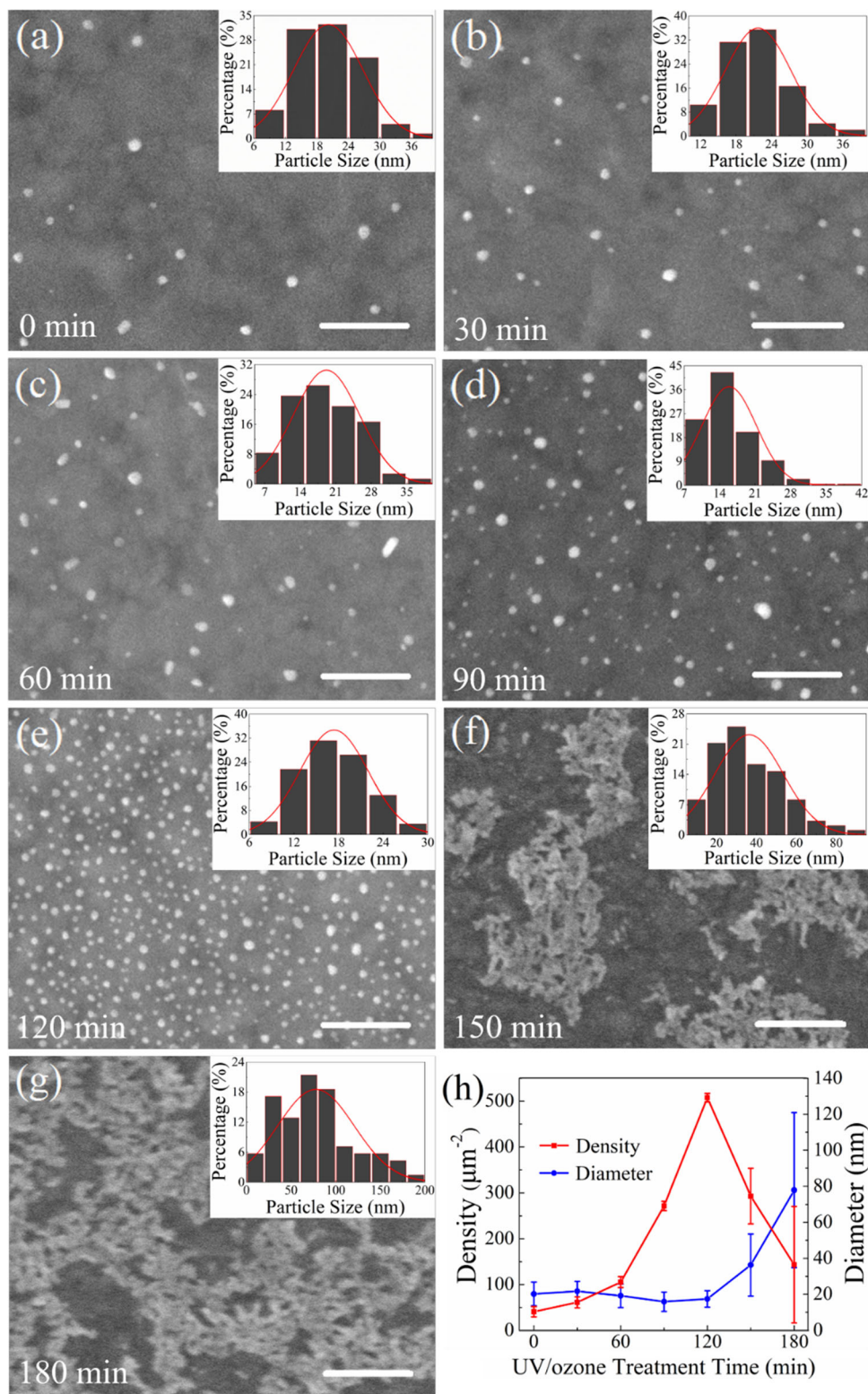
To further characterize AuNPs and the elemental distributions of AuNPs/RGO nanocomposites after 120 min UV/ozone treatment (S4), TEM measurement was performed. Figure 3a shows the TEM image of AuNPs/RGO at low magnification. The AuNPs exhibited roughly spherical shape and were uniformly distributed on the RGO surface with a very high loading. The high-resolution TEM (HRTEM) image of a single AuNP is distinctly presented in Fig. 3b, where the lattice fringes can be clearly seen. The lattice spacing was measured to be 0.238 nm, which coincides well with Au (111) (JCPDS 04-0784). Electron energy loss spectroscopy (EELS) elemental mapping (Fig. 3c) and energy-dispersive X-ray spectroscopy (EDS) spectrum (Fig. 3d) further confirm the presence and uniform distribution of AuNPs on the RGO sheets.

Under the optimal condition (i.e., UV/ozone exposure of GO for 120 min), the AuNPs/RGO/Au plasmonic nano-sandwiches with an upper layer of high-density, good-dispersity and aggregation-free AuNPs were successfully prepared. More importantly, compared with other methods proposed previously for fabricating metal NP/graphene nanocomposites at room temperature (see Table 3), the strategy presented here offers a new route to achieving much denser metal NPs on graphene, while alleviate the etching effect of plasma at the same time, which is helpful in averting severe damage to graphene.

Enhanced SERS in AuNPs/RGO/Au

Enhancing the local electric field in graphene-based plasmonic nanostructures has been demonstrated as an effective way to improve the efficiency of various electro-optic processes [46], and graphene is an advantageous test bed for studying the mechanisms of optical response in plasmonic nanostructures

Figure 2 FESEM images of AuNPs on the surface of RGO that were treated with UV/ ozone for **a** 0 min, **b** 30 min, **c** 60 min, **d** 90 min, **e** 120 min, **f** 150 min and **g** 180 min, respectively. The scale bar is 200 nm. Size-distribution histograms of AuNPs are shown in the insets of (a–g). **h** The density and size of AuNPs as a function of UV/ozone treatment time.



[10, 47–50]. We performed Raman measurements for GO spin-coated on SiO_2/Si , GO spin-coated on $\text{Au}/\text{SiO}_2/\text{Si}$ and AuNPs/RGO/Au nano-sandwiches and the spectra are shown in Fig. 4. The band intensities

in pristine GO on SiO_2/Si were rather weak with the intensity of G band being less than 200 counts. While the intensity of G band was slightly enhanced (ca. fourfold) on Au film, a remarkable enhancement of G

Figure 3 Structural and elemental analyses of AuNPs/RGO nanocomposites treated with UV/ozone for 120 min (S4). **a** Low-magnified TEM image of AuNPs/RGO nanocomposites. **b** HRTEM image of AuNPs/RGO. **c** The corresponding EELS element mapping of AuNPs/RGO. **d** The EDS spectrum measured during the TEM analysis.

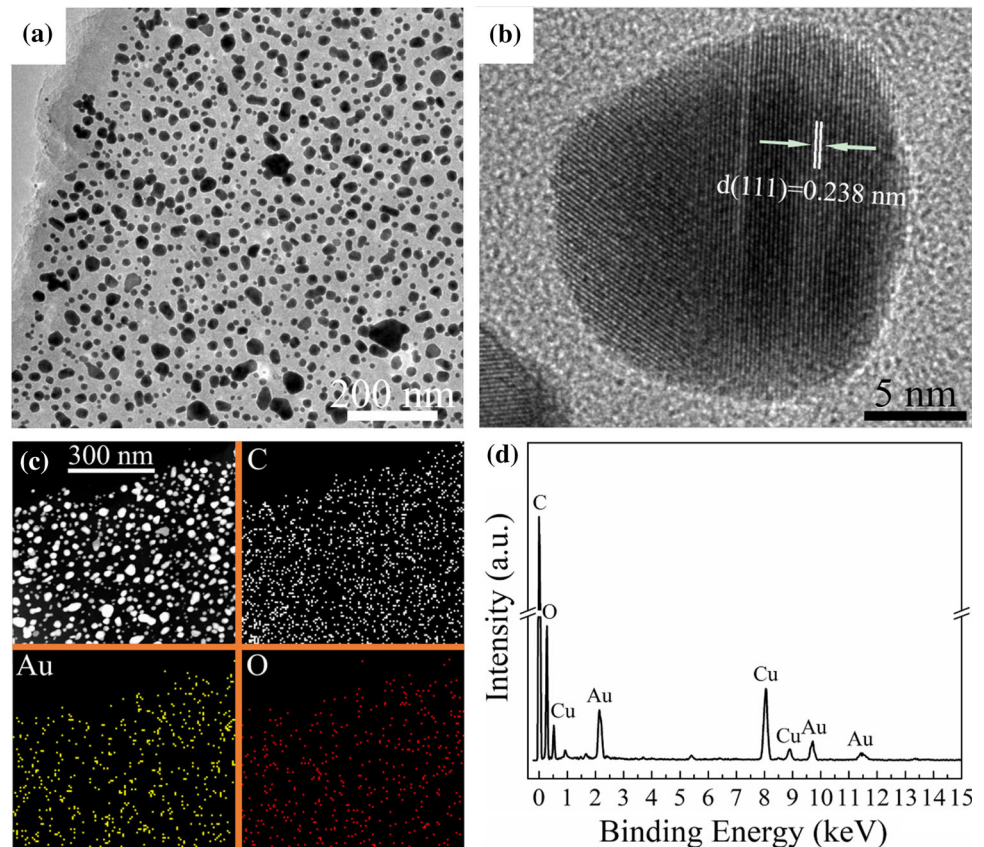


Table 3 A NP density comparison of graphene-based metal-NPs nanocomposites fabricated at room-temperature with different synthetic methods

Nanocomposites	Synthetic methods	Density (μm^{-2})	Year	Ref
AuNP/graphene	Chemical reduction	18	2013	[24]
AgNP-graphene-AgNP	Self-assembly	120	2015	[22]
AuNPs/GO	Self-assembly	~ 60	2017	[21]
AuNPs/RGO/Au	UV/ozone functionalization and Ar plasma reduction	508	2020	This work

band was observed in AuNPs/RGO/Au nano-sandwiches with the enhancement factor for G band exceeding 300. The significant enhancement can be attributed to the multiple plasmonic couplings including the AuNP–AuNP coupling and AuNP–Au film coupling constructed by intercalating RGO as a nano-spacer [13], and the satisfactory enhancement ratio is comparable to the highest ones observed in graphene-embedded plasmonic nanostructures reported to date [13, 15, 51–53]. Moreover, the strong multiple plasmonic couplings also contribute predominantly to the AuNPs/RGO/Au nano-sandwich system when used as a sensitive analyte-detection

platform, which will be discussed below. Besides, compared with previous studies that achieved high-density plasmonic NPs through annealing metal thin film at high temperatures to gain ultrahigh enhancement of local electric field [15, 52, 53], our UV/ozone-assisted synthetic strategy shows its superiority by offering satisfactory enhancement with all the fabrication procedures being carried out at room temperature, which makes this strategy compatible with flexible optoelectronics.

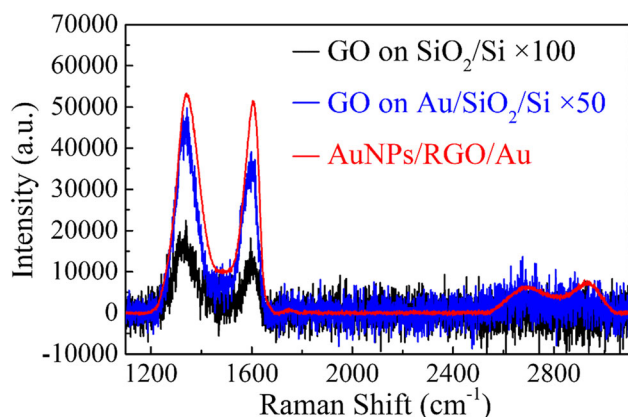


Figure 4 Raman spectra of GO on SiO₂/Si (black line), GO on Au/SiO₂/Si (blue line) and AuNPs/RGO/Au (red line).

SERS performance of AuNPs/RGO/Au nano-sandwiches

R6G, one of the widely used standard probe molecules for the evaluation of SERS properties, was chosen to assess the performance of our AuNPs/RGO/Au plasmonic nano-sandwiches as SERS substrates. The Raman spectra of R6G on substrate S0–S6 are presented in Fig. 5a. The strong Raman peaks at 611 cm⁻¹, 771 cm⁻¹, 1089 cm⁻¹, 1124 cm⁻¹, 1183 cm⁻¹, 1309 cm⁻¹, 1361 cm⁻¹, 1508 cm⁻¹, 1572 cm⁻¹, 1597 cm⁻¹ and 1648 cm⁻¹ are in good agreement with the literature [54]. Figure 5b indicates the characteristic Raman shift peak intensity at 611 cm⁻¹ as a function of UV/ozone treatment time. The intensity of Raman signal exhibits a clear volcano-type trend with the increase in treatment time, which matches with the trend of particle density. The overlap of these two curves is due to the positive correlation between the particle density and the number of “hot spots” [55, 56] for SERS. In order to evaluate the reproducibility of Raman spectra of R6G on our optimal sample, Raman measurements were performed at 20 randomly selected spots on the substrate S4, and the peak intensities at 611 cm⁻¹ are shown in Fig. 5c. The relative standard deviation (RSD) of peak intensities centered at 611 cm⁻¹ was calculated to be 6.1%, demonstrating high homogeneity of our plasmonic substrates and good reproducibility of Raman spectra. To assess the linear dependence of SERS signal intensity on the concentration of R6G molecules and the limit of detection of the substrate S4, a series of Raman spectra at different concentration were obtained. A broad range of linear

response from 5×10^{-5} to 5×10^{-8} M with a detection limit of around 5×10^{-8} M was achieved ($R^2 = 0.9954$) without the aid of digital mapping, as illustrated in Fig. 5d. Furthermore, the detection limit of R6G on the optimum AuNPs/RGO/Au nano-sandwich (S4) was compared with that on bare SiO₂/Si, as shown in Fig. 5e, and a substantial enhancement of detection limit can be seen. The peak intensity of 611 cm⁻¹ band of 5×10^{-8} M R6G on AuNPs/RGO/Au/SiO₂/Si is 461 counts and the peak intensity of 611 cm⁻¹ band of 1×10^{-3} M R6G on SiO₂/Si is 352. We used the standard equation $EF = \frac{I_{SERS}}{I_{bulk}} \times \frac{N_{bulk}}{N_{SERS}}$ [57] to calculate the enhancement factor (EF). I_{SERS} and I_{bulk} are the peak intensity of 611 cm⁻¹ band of 5×10^{-8} M R6G on the plasmonic substrate and 1×10^{-3} M R6G on the bare substrate, respectively, and N_{SERS} and N_{bulk} are the number of R6G molecules excited by the Raman laser beam on the plasmonic and bare substrates, respectively. Since the laser power was fixed at 1.7 mW in all measurements, the activated volume was assumed to be identical, which means the value of $\frac{N_{bulk}}{N_{SERS}}$ equals to that of $\frac{C_{bulk}}{C_{SERS}}$. In our work, I_{SERS} , I_{bulk} , C_{bulk} , C_{SERS} equals to 461 counts, 352 counts, 1×10^{-3} M and 5×10^{-8} M, respectively, and the EF is therefore calculated to be 2.6×10^4 . A comparison of the limit of detection (LOD) and EF of Rhodamine 6G on different graphene-based plasmonic nanostructures is listed in Table 4. The LOD in our work is comparable with the values reported in prior work, but the EF value is limited due to the following reasons. Firstly, the Raman laser wavelength does not match with the resonance wavelength of our plasmonic nano-sandwiches. Secondly, owing to overlap between bands of R6G and GO at ~ 1350 cm⁻¹, we had to use 611 cm⁻¹ band of R6G to determine the EF and LOD, which partially results in relatively lower EF and LOD [66]. Last but not least, because the plasmonic coupling between two metal layers decays as the number of graphene layer increases [53, 69], the use of few-layer RGO instead of single-layer RGO as the intercalation layer also leads to a decrease in EF.

The stability performance is shown in Fig. 5f. We carried out Raman measurements of R6G on both a fresh substrate and an aged one stored under ambient conditions for 30 days. Compared with the Raman spectrum on the fresh substrate, the Raman spectrum on the aged one shows identical Raman fingerprint bands with an intensity loss at 611 cm⁻¹

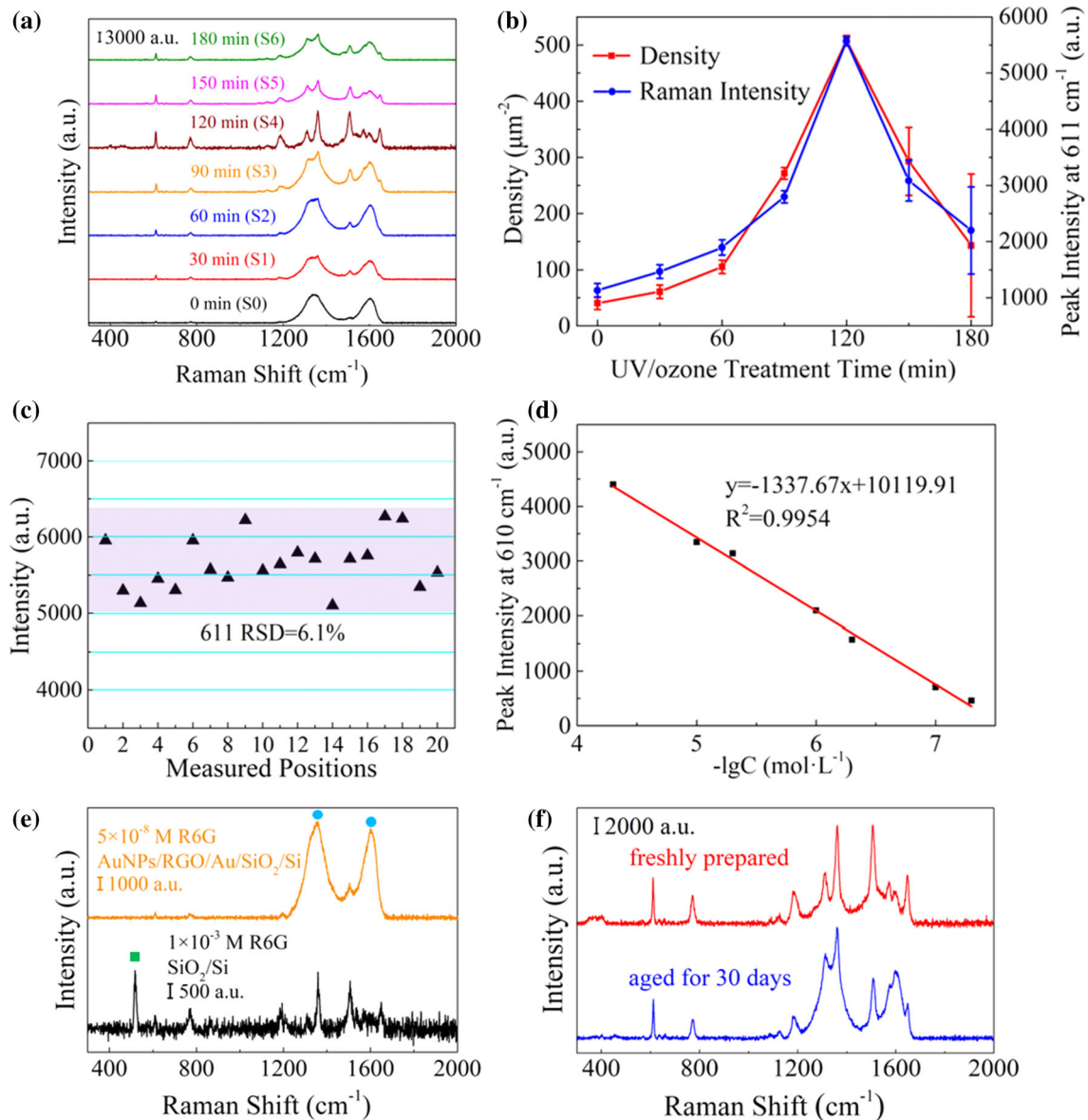


Figure 5 **a** Raman spectra of R6G on S0, S1, S2, S3, S4, S5 and S6, respectively. **b** The change of characteristic Raman shift peak intensity at 611 cm^{-1} of R6G and density of AuNPs as a function of UV/ozone treatment time. **c** Variation of peak intensities of the 611 cm^{-1} bands in Raman spectra collected from 20 randomly selected spots on substrate S4. **d** The intensity of the Raman feature peak of the R6G at 611 cm^{-1} as a function of molecular

concentration from 5×10^{-5} to $5 \times 10^{-8} \text{ M}$ using substrate S4. **e** Raman spectra of $1 \times 10^{-3} \text{ M}$ R6G on SiO₂/Si and $5 \times 10^{-8} \text{ M}$ R6G on AuNPs/RGO/Au nano-sandwiches, respectively. **f** Raman spectra of $1 \times 10^{-4} \text{ M}$ R6G on a freshly substrate and an aged one stored under ambient conditions for 30 days. The symbol “blue solid circle” and “green solid square” denote characteristic Raman shift peaks of GO and SiO₂.

of only 3.7%. Since UV/ozone treatment induces epoxide formation on the basal plane of GO, we believe that the loss of stability is caused by restacking of RGO due to linking of discrete RGO layers by hydrogen bonding between oxygen atoms of epoxides and adsorbed water molecules from ambient air [70], which weakens the plasmonic coupling between Au film and AuNPs [53, 69].

Conclusions

In summary, we have developed a facile yet efficient approach to fabricating AuNPs/RGO/Au plasmonic nano-sandwiches with good tunability of AuNPs at room temperature with the aid of UV/ozone treatment. Combining the results from XPS and Raman analyses, we conclude that, the oxygen-

Table 4 A comparison of the limit of detection and enhancement factor of Rhodamine 6G on different graphene-based plasmonic nanostructures

Structure	Limit of detection (M)	Enhancement factor at 611 cm ⁻¹ band	Enhancement factor at 1361 cm ⁻¹ band	Fabrication method	Year	Ref
AgNPs/SLRGO ¹	1 × 10 ⁻⁸	N/A	N/A	Chemical reduction	2011	[58]
AgNPs/RGO	1 × 10 ⁻⁸	N/A	N/A	Chemical reduction	2013	[59]
SLG/AuNPs ²	1 × 10 ⁻⁸	~ 10 ⁷	N/A	Self-assembly	2014	[60]
GO/Ag octahedron	1 × 10 ⁻⁹	N/A	N/A	Self-assembly	2014	[61]
AuNPs/SLG/ AuNPs	1 × 10 ⁻⁹	2.5 × 10 ⁸	N/A	Vacuum deposition	2014	[53]
FLG/AgNPs/FLG ³	1 × 10 ⁻⁸	N/A	2.4 × 10 ⁷	Self-assembly	2015	[62]
Au nanorods/cysteine- GO	5 × 10 ⁻⁶	N/A	8.6 × 10 ⁴	Self-assembly	2016	[63]
AuNPs/graphene	8 × 10 ⁻⁷	N/A	N/A	E-beam evaporation	2017	[64]
AgNPs/GO	1 × 10 ⁻⁷	4.8 × 10 ⁶	N/A	Chemical reduction	2017	[65]
AuNPs/wrinkled graphene	1 × 10 ⁻⁹	6.4 × 10 ⁶	1.2 × 10 ⁷	E-beam evaporation	2017	[66]
AuNPs/graphene	5 × 10 ⁻⁹	N/A	N/A	E-beam evaporation	2020	[67]
Au nanodot arrays/ SLG	1 × 10 ⁻¹²	N/A	8.8 × 10 ⁸	E-beam evaporation	2020	[68]
AuNPs/RGO/Au	5 × 10 ⁻⁸	2.6 × 10 ⁴	N/A	Plasma treatment	2020	This work

¹SLRGO single-layer reduced graphene oxide, ²SLG single-layer graphene, ³FLG few-layer graphene

functionalization of GO during the UV/ozone treatment process is ascribed to the formation of epoxide groups and oxidation of hydroxyl into carboxyl. Notably, the oxygen-containing functional groups, which were generally associated with negative contributions, were successfully utilized to readily tune the nucleation and growth processes of AuNPs on the surfaces of RGO. By optimizing UV/ozone treatment time length, the plasmonic nano-sandwiches with an upper layer of high-density, good-dispersity and aggregation-free AuNPs were successfully synthesized. The resultant AuNPs/RGO/Au plasmonic nano-sandwiches offer considerable near-field enhancement with a graphene Raman enhancement factor of over 300. The as-fabricated nano-sandwiches exhibit good performance when used as SERS substrates. It is expected that this work will not only offer an effective strategy for the synthesis of graphene-based plasmonic nanostructures in the field of

flexible electronics, but also holds the potential to be extended to other areas that entail metal nanoparticle/RGO such as catalysis (e.g., hydrogen evolution reaction), fuel cells and actuators.

Acknowledgements

The authors would like to thank Dr. Yi Wan from Fudan University for the kind assistance for Raman measurements. This work was supported by the National Natural Science Foundation of China (51677031, 11975081, 61705042).

Compliance with ethical standards

Conflict of interest The authors declare no conflict of interest.

Electronic supplementary material: The online version of this article (<https://doi.org/10.1007/s10853-020-05376-x>) contains supplementary material, which is available to authorized users.

References

- [1] Zhao Y, Zhu Y (2015) Graphene-based hybrid films for plasmonic sensing. *Nanoscale* 7(35):14561–14576
- [2] Dou S, Tao L, Wang R, El Hankari S, Chen R, Wang S (2018) Plasma-assisted synthesis and surface modification of electrode materials for renewable energy. *Adv Mater* 30(21):1705850
- [3] Das S, Pandey D, Thomas J, Roy T (2019) The role of graphene and other 2D materials in solar photovoltaics. *Adv Mater* 31(1):1802722
- [4] Wu J, Lu Y, Feng S, Wu Z, Lin S, Hao Z, Yao T, Li X, Zhu H, Lin S (2018) The interaction between quantum dots and graphene: the applications in graphene-based solar cells and photodetectors. *Adv Funct Mater* 28(50):1804712
- [5] Xu G-R, Hui J-J, Huang T, Chen Y, Lee J-M (2015) Platinum nanocuboids supported on reduced graphene oxide as efficient electrocatalyst for the hydrogen evolution reaction. *J Power Sources* 285:393–399
- [6] Yu X, Kuai L, Geng B (2012) CeO₂/rGO/Pt sandwich nanostructure: rGO-enhanced electron transmission between metal oxide and metal nanoparticles for anodic methanol oxidation of direct methanol fuel cells. *Nanoscale* 4(18):5738–5743
- [7] Lu L, Liu J, Hu Y, Zhang Y, Chen W (2013) Graphene-stabilized silver nanoparticle electrochemical electrode for actuator design. *Adv Mater* 25(9):1270–1274
- [8] Echtermeyer TJ, Britnell L, Jasnos PK, Lombardo A, Gorbachev RV, Grigorenko AN, Geim AK, Ferrari AC, Novoselov KS (2011) Strong plasmonic enhancement of photovoltage in graphene. *Nat Commun* 2:458
- [9] Chen Z, Li X, Wang J, Tao L, Long M, Liang SJ, Ang LK, Shu C, Tsang HK, Xu JB (2017) Synergistic effects of plasmonics and electron trapping in graphene short-wave infrared photodetectors with ultrahigh responsivity. *ACS Nano* 11(1):430–437
- [10] Xu G, Liu J, Wang Q, Hui R, Chen Z, Maroni VA, Wu J (2012) Plasmonic graphene transparent conductors. *Adv Mater* 24(10):OP71–OP76
- [11] Zhang PY, Song T, Wang TT, Zeng HP (2018) Plasmonic Cu nanoparticle on reduced graphene oxide nanosheet support: an efficient photocatalyst for improvement of near-infrared photocatalytic H₂ evolution. *Appl Catal B-Environ* 225:172–179
- [12] Kirubasankar B, Murugadoss V, Lin J, Ding T, Dong MY, Liu H, Zhang JX, Li TX, Wang N, Guo ZH, Angaiah S (2018) In situ grown nickel selenide on graphene nanohybrid electrodes for high energy density asymmetric supercapacitors. *Nanoscale* 10(43):20414–20425
- [13] Li X, Choy WCH, Ren X, Zhang D, Lu H (2014) Highly intensified surface enhanced Raman scattering by using monolayer graphene as the nanospacer of metal film-metal nanoparticle coupling system. *Adv Funct Mater* 24(21):3114–3122
- [14] Lee KJ, Kim D, Jang BC, Kim D-J, Park H, Jung DY, Hong W, Kim TK, Choi Y-K, Choi S-Y (2016) Multilayer graphene with a rippled structure as a spacer for improving plasmonic coupling. *Adv Funct Mater* 26(28):5093–5101
- [15] Zhan Z, Liu L, Wang W, Cao Z, Martinelli A, Wang E, Cao Y, Chen J, Yurgens A, Sun J (2016) Ultrahigh surface-enhanced Raman scattering of graphene from Au/Graphene/Au sandwiched structures with subnanometer gap. *Adv Opt Mater* 4(12):2021–2027
- [16] Koppens FH, Chang DE, Garcia de Abajo FJ (2011) Graphene plasmonics: a platform for strong light-matter interactions. *Nano Lett* 11(8):3370–3377
- [17] Grigorenko AN, Polini M, Novoselov KS (2012) Graphene plasmonics. *Nat Photonics* 6(11):749–758
- [18] Huang X, Qi X, Boey F, Zhang H (2012) Graphene-based composites. *Chem Soc Rev* 41(2):666–686
- [19] Singh V, Joung D, Zhai L, Das S, Khondaker SI, Seal S (2011) Graphene based materials: past, present and future. *Prog Mater Sci* 56(8):1178–1271
- [20] Huang J, Zhang L, Chen B, Ji N, Chen F, Zhang Y, Zhang Z (2010) Nanocomposites of size-controlled gold nanoparticles and graphene oxide: formation and applications in SERS and catalysis. *Nanoscale* 2(12):2733–2738
- [21] Li Y, Yang J, Zhou Y, Zhao N, Zeng W, Wang W (2017) Fabrication of gold nanoparticles/graphene oxide films with surface-enhanced Raman scattering activity by a simple electrostatic self-assembly method. *Colloid Surf A* 512:93–100
- [22] Wu J, Xu Y, Xu P, Pan Z, Chen S, Shen Q, Zhan L, Zhang Y, Ni W (2015) Surface-enhanced Raman scattering from AgNP-graphene-AgNP sandwiched nanostructures. *Nanoscale* 7(41):17529–17537
- [23] Muszynski R, Seger B, Kamat PV (2008) Decorating graphene sheets with gold nanoparticles. *J Phys Chem C* 112(14):5263–5266
- [24] Lee S, Lee MH, Shin H-J, Choi D (2013) Control of density and LSPR of Au nanoparticles on graphene. *Nanotechnology* 24(27):275702

- [25] Zhou H, Qiu C, Liu Z, Yang H, Hu L, Liu J, Yang H, Gu C, Sun L (2010) Thickness-dependent morphologies of gold on n-layer graphenes. *J Am Chem Soc* 132(3):944–946
- [26] Takahashi S, Chiba H, Kato T, Endo S, Hayashi T, Todoroki N, Wadayama T (2015) Oxygen reduction reaction activity and structural stability of Pt–Au nanoparticles prepared by arc-plasma deposition. *Phys Chem Chem Phys* 17(28):18638–18644
- [27] Yang C, Yu Y, Xie YJ, Zhang D, Zeng P, Dong YR, Yang BL, Liang RQ, Ou QR, Zhang SY (2019) One-step synthesis of size-tunable gold nanoparticles/reduced graphene oxide nanocomposites using argon plasma and their applications in sensing and catalysis. *Appl Surf Sci* 473:83–90
- [28] Wang Q, Song M, Chen C, Hu W, Wang X (2012) Plasma synthesis of surface-functionalized graphene-based platinum nanoparticles: highly active electrocatalysts as electrodes for direct methanol fuel cells. *ChemPlusChem* 77(6):432–436
- [29] Su N, Hu X, Zhang J, Huang H, Cheng J, Yu J, Ge C (2017) Plasma-induced synthesis of Pt nanoparticles supported on TiO₂ nanotubes for enhanced methanol electro-oxidation. *Appl Surf Sci* 399:403–410
- [30] Gong X, Liu G, Li Y, Yu DYW, Teoh WY (2016) Functionalized-graphene composites: fabrication and applications in sustainable energy and environment. *Chem Mater* 28(22):8082–8118
- [31] Ma Y, Fang S, Wang Q (2017) The tunable plasma synthesis of Pt-reduced graphene oxide nanocomposites. *AIP Adv* 7(6):065118
- [32] Wang Q, Zuo X, Wang X (2014) Preparation of graphene supported Pt nanoparticles by a plasma approach and their application for methanol electro-oxidation: a comparison with chemical reduction. *Dalton Trans* 43(34):12961–12966
- [33] Yang C, Gong J, Zeng P, Yang X, Liang R, Ou Q, Zhang S (2018) Fast room-temperature reduction of graphene oxide by methane/argon plasma for flexible electronics. *Appl Surf Sci* 452:481–486
- [34] Paredes JI, Villar-Rodil S, Solis-Fernandez P, Martinez-Alonso A, Tascon JM (2009) Atomic force and scanning tunneling microscopy imaging of graphene nanosheets derived from graphite oxide. *Langmuir* 25(10):5957–5968
- [35] Singh G, Botcha VD, Sutar DS, Narayanam PK, Talwar SS, Srinivasa RS, Major SS (2014) Near room temperature reduction of graphene oxide Langmuir–Blodgett monolayers by hydrogen plasma. *Phys Chem Chem Phys* 16(23):11708–11718
- [36] Palchan I, Crespin M, Estrade-Szwarczopf H, Rousseau B (1989) Graphite fluorides: an XPS study of a new type of C–F bonding. *Chem Phys Lett* 157(4):321–327
- [37] Lee G, Lee B, Kim J, Cho K (2009) Ozone adsorption on graphene: Ab initio study and experimental validation. *J Phys Chem C* 113(32):14225–14229
- [38] Lee B, Park S-Y, Kim H-C, Cho K, Vogel EM, Kim MJ, Wallace RM, Kim J (2008) Conformal Al₂O₃ dielectric layer deposited by atomic layer deposition for graphene-based nanoelectronics. *Appl Phys Lett* 92(20):203102
- [39] Checa M, Figueredo M, Aguinaco A, Beltran FJ (2019) Graphene oxide/titania photocatalytic ozonation of primidone in a visible LED photoreactor. *J Hazard Mater* 369:70–78
- [40] Huh S, Park J, Kim YS, Kim KS, Hong BH, Nam J-M (2011) UV/ozone-oxidized large-scale graphene platform with large chemical enhancement in surface-enhanced Raman scattering. *ACS Nano* 5(12):9799–9806
- [41] Kwon KC, Dong WJ, Jung GH, Ham J, Lee J-L, Kim SY (2013) Extension of stability in organic photovoltaic cells using UV/ozone-treated graphene sheets. *Sol Energy Mater Sol Cells* 109:148–154
- [42] Lucchese MM, Stavale F, Ferreira EHM, Vilani C, Moutinho MVO, Capaz RB, Achete CA, Jorio A (2010) Quantifying ion-induced defects and Raman relaxation length in graphene. *Carbon* 48(5):1592–1597
- [43] Cancado LG, Jorio A, Ferreira EH, Stavale F, Achete CA, Capaz RB, Moutinho MV, Lombardo A, Kulmala TS, Ferrari AC (2011) Quantifying defects in graphene via Raman spectroscopy at different excitation energies. *Nano Lett* 11(8):3190–3196
- [44] Jorio A, Lucchese MM, Stavale F, Ferreira EH, Moutinho MV, Capaz RB, Achete CA (2010) Raman study of ion-induced defects in N-layer graphene. *J Phys: Condens Matter* 22(33):334204
- [45] Xu W, Wang X, Zhou Q, Meng B, Zhao J, Qiu J, Gogotsi Y (2012) Low-temperature plasma-assisted preparation of graphene supported palladium nanoparticles with high hydrodesulfurization activity. *J Mater Chem* 22(29):14363–14368
- [46] Schedin F, Lidorikis E, Lombardo A, Kravets VG, Geim AK, Grigorenko AN, Novoselov KS, Ferrari AC (2010) Surface-enhanced Raman spectroscopy of graphene. *ACS Nano* 4(10):5617–5626
- [47] Tian H, Chen H-Y, Gao B, Yu S, Liang J, Yang Y, Xie D, Kang J, Ren T-L, Zhang Y, Wong HSP (2013) Monitoring oxygen movement by Raman spectroscopy of resistive random access memory with a graphene-inserted electrode. *Nano Lett* 13(2):651–657
- [48] Ling X, Xie L, Fang Y, Xu H, Zhang H, Kong J, Dresselhaus MS, Zhang J, Liu Z (2010) Can graphene be used as a substrate for Raman enhancement? *Nano Lett* 10(2):553–561

- [49] Thrall ES, Crowther AC, Yu Z, Brus LE (2012) R6G on graphene: high Raman detection sensitivity, yet decreased Raman cross-section. *Nano Lett* 12(3):1571–1577
- [50] Kravets VG, Schedin F, Jalil R, Britnell L, Novoselov KS, Grigorenko AN (2012) Surface hydrogenation and optics of a graphene sheet transferred onto a plasmonic nanoarray. *J Phys Chem C* 116(6):3882–3887
- [51] Wang P, Zhang W, Liang O, Pantoja M, Katzer J, Schroeder T, Xie YH (2012) Giant optical response from graphene–plasmonic system. *ACS Nano* 6(7):6244–6249
- [52] Xu W, Xiao J, Chen Y, Chen Y, Ling X, Zhang J (2013) Graphene-veiled gold substrate for surface-enhanced Raman spectroscopy. *Adv Mater* 25(6):928–933
- [53] Zhao Y, Li X, Du Y, Chen G, Qu Y, Jiang J, Zhu Y (2014) Strong light-matter interactions in sub-nanometer gaps defined by monolayer graphene: toward highly sensitive SERS substrates. *Nanoscale* 6(19):11112–11120
- [54] Lu R, Konzelmann A, Xu F, Gong Y, Liu J, Liu Q, Xin M, Hui R, Wu JZ (2015) High sensitivity surface enhanced Raman spectroscopy of R6G on in situ fabricated Au nanoparticle/graphene plasmonic substrates. *Carbon* 86:78–85
- [55] Schlucker S (2014) Surface-enhanced Raman spectroscopy: concepts and chemical applications. *Angew Chem Int Ed* 53(19):4756–4795
- [56] Xu H, Aizpurua J, Käll M, Apell P (2000) Electromagnetic contributions to single-molecule sensitivity in surface-enhanced Raman scattering. *Phys Rev E* 62(3):4318–4324
- [57] Wustholz KL, Brosseau CL, Casadio F, Van Duyne RP (2009) Surface-enhanced Raman spectroscopy of dyes: from single molecules to the artists' canvas. *Phys Chem Chem Phys* 11(34):7350–7359
- [58] Lu G, Li H, Liusman C, Yin Z, Wu S, Zhang H (2011) Surface enhanced Raman scattering of Ag or Au nanoparticle-decorated reduced graphene oxide for detection of aromatic molecules. *Chem Sci* 2(9):1817–1821
- [59] Li SK, Yan YX, Wang JL, Yu SH (2013) Bio-inspired in situ growth of monolayer silver nanoparticles on graphene oxide paper as multifunctional substrate. *Nanoscale* 5(24):12616–12623
- [60] Du Y, Zhao Y, Qu Y, Chen C-H, Chen C-M, Chuang C-H, Zhu Y (2014) Enhanced light-matter interaction of graphene–gold nanoparticle hybrid films for high-performance SERS detection. *J Mater Chem C* 2(23):4683–4691
- [61] Fan W, Lee YH, Pedireddy S, Zhang Q, Liu T, Ling XY (2014) Graphene oxide and shape-controlled silver nanoparticle hybrids for ultrasensitive single-particle surface-enhanced Raman scattering (SERS) sensing. *Nanoscale* 6(9):4843–4851
- [62] Gong T, Zhu Y, Zhang J, Ren W, Quan J, Wang N (2015) Study on surface-enhanced Raman scattering substrates structured with hybrid Ag nanoparticles and few-layer graphene. *Carbon* 87:385–394
- [63] Cao X, Yan S, Cheng Y, Wang J, Zhu Y, Sun B, Xiao Z (2016) Cysteine-modified Graphene/Gold nanorod composites toward rhodamine 6G detection by surface-enhanced Raman scattering. *J Nanosci Nanotechnol* 16(7):6697–6704
- [64] Goul R, Das S, Liu Q, Xin M, Lu R, Hui R, Wu JZ (2017) Quantitative analysis of surface enhanced Raman spectroscopy of Rhodamine 6G using a composite graphene and plasmonic Au nanoparticle substrate. *Carbon* 111:386–392
- [65] Liang X, Liang B, Pan Z, Lang X, Zhang Y, Wang G, Yin P, Guo L (2015) Tuning plasmonic and chemical enhancement for SERS detection on graphene-based Au hybrids. *Nanoscale* 7(47):20188–20196
- [66] Chen W, Gui X, Zheng Y, Liang B, Lin Z, Zhao C, Chen H, Chen Z, Li X, Tang Z (2017) Synergistic effects of wrinkled graphene and plasmonics in stretchable hybrid platform for surface-enhanced Raman spectroscopy. *Adv Opt Mater* 5(6):1600715
- [67] Ghopry SA, Alamri M, Goul R, Cook B, Sadeghi SM, Gutha RR, Sakidja R, Wu JZ (2020) Au Nanoparticle/WS₂ Nanodome/Graphene van der Waals heterostructure substrates for surface-enhanced Raman spectroscopy. *ACS Appl Nano Mater* 3(3):2354–2363
- [68] Sivashanmugan K, Nguyen V-H, Nguyen B-S (2020) Tailoring a novel Au nanodot arrays on graphene substrate for a highly active surface-enhanced Raman scattering (SERS). *Mater Lett* 271:127807
- [69] Zhao Y, Yang D, Li X, Liu Y, Hu X, Zhou D, Lu Y (2017) Toward highly sensitive surface-enhanced Raman scattering: the design of a 3D hybrid system with monolayer graphene sandwiched between silver nanohole arrays and gold nanoparticles. *Nanoscale* 9(3):1087–1096
- [70] Dreyer DR, Park S, Bielawski CW, Ruoff RS (2010) The chemistry of graphene oxide. *Chem Soc Rev* 39(1):228–240

Publisher's Note Springer Nature remains neutral with regard to jurisdictional claims in published maps and institutional affiliations.